Performance Analysis of a High-Temperature Kalina Cycle Integrated with Parabolic Trough Collectors for CSP in México

Eduardo González-Mora[1]

[1] Ingeniería en Sistemas Energéticos Sustentables, Facultad de Ingeniería, Universidad Autónoma del Estado de México, Toluca (México)

Abstract

Concentrated solar power (CSP) converts sunlight into heat for mechanical or electrical energy generation, offering a dispatchable alternative to variable renewables and often integrating thermal energy storage (TES) to extend power delivery beyond daylight hours. The Kalina cycle, employing an ammonia–water working fluid, enables variable-temperature heat exchange and reduces exergy losses compared with conventional Rankine-based systems; however, its application in CSP remains limited. This study evaluates the feasibility of a 10 MW high-temperature Kalina cycle (HT-KC) coupled to a parabolic trough collector (PTC) field and molten-salt TES under real-world Mexican solar conditions. Through exergy-efficiency optimization via the Variable Metric Method and solar-field sizing at a solar multiple of 1.5 for the 21 June design point, the HT-KC achieves a first-law efficiency of 32.51% and an exergy efficiency of 66.4% under design-day conditions, attains an annual solar fraction of 41.87%, and maintains a capacity factor of 44.10%. Compared with a 10 MW direct-steam-generation Rankine benchmark—which delivers higher peak efficiencies (26% energy, 35% exergy) but requires larger fields and lacks cost-effective storage—the HT-KC demonstrates superior dispatchability and operational flexibility. These results provide a rigorous framework for designing reliable renewable power systems in high-irradiance regions and support strategic planning for grid-stable decarbonization.

Keywords: CSP, High-temperature Kalina cycle, Thermal efficiency, TES, Exergy

1. Introduction

Concentrated solar power (CSP) offers a reliable and dispatchable pathway for decarbonizing electricity generation by converting concentrated sunlight into high-temperature thermal energy. Unlike photovoltaic or wind technologies, CSP systems employ optical concentrators—typically mirrors or Fresnel lenses—to focus solar radiation onto a receiver, producing heat to drive thermodynamic cycles. A key advantage of CSP lies in its seamless integration with thermal energy storage (TES), most commonly based on molten salts. This storage enables multi-hour retention of excess thermal energy, supporting electricity production during non-solar periods and meeting peak grid demand (Prieto et al., 2024). By addressing the intermittency limitations of other renewables, CSP contributes directly to grid flexibility and stability (Lovegrove and Stein, 2021).

Among advanced power cycles considered for CSP integration, the Kalina cycle (KC) has demonstrated superior thermodynamic performance over conventional Rankine and Organic Rankine Cycles (ORCs). The KC utilizes an ammonia–water mixture as its working fluid, enabling non-isothermal phase change during evaporation and condensation. This variable-temperature heat transfer mechanism significantly reduces exergy destruction across heat exchangers, making the KC particularly well-suited for fluctuating and medium-grade heat sources typical of solar thermal systems. Comparative studies report thermal efficiency improvements of 10–50% over ORC systems under similar conditions. For instance, in waste heat recovery applications, the KC achieves energy efficiencies of 21.13% compared to 19.02% for ORCs, with corresponding exergy efficiencies of 49.88% and 45.08%, respectively. Additionally, the Kalina cycle exhibits a higher exergetic sustainability index (0.60–1.34) and emits 32% less CO_2 (4.49 kg/h) than comparable ORCs—features aligned with the decarbonization goals of modern thermal infrastructure(Bandhan et al., 2024; Elbir, 2024; Jeannot et al., 2021; Nemati et al., 2017).

Despite its thermodynamic advantages, the Kalina cycle remains underutilized in CSP applications, especially

10.18086/swc.2025.01.17 Available at http://proceedings.ises.org

at high temperatures and with TES integration, due to modeling complexity, material compatibility issues, and limited demonstration projects. These limitations are particularly relevant in Mexico, where fossil fuels dominate the electricity matrix, contributing 76.81% of national generation (NREL, 2023; SENER, 2023a, 2023b). olar energy represents just 5.2% of the mix, primarily from photovoltaic systems, with only one CSP facility in operation: the Agua Prieta II integrated solar combined cycle (ISCC) plant. Of its 476.4 MW net capacity, just 12 MW is attributable to its parabolic trough solar field (NREL, 2023; SENER, 2017).

To meet its national target of 35% renewable energy, Mexico must significantly expand CSP capacity while improving the efficiency and adaptability of solar thermal systems. This expansion demands thermodynamic models that go beyond conventional energy balances to include exergy-based assessments, which quantify the quality and usability of energy and identify system irreversibilities. Moreover, CSP projects in Mexico must account for regional constraints such as arid climate, high direct normal irradiance (DNI) variability, and water scarcity. The ammonia–water mixture used in the KC reduces cooling water demand and offers high efficiency under varying heat inputs, making it a promising solution over the steam Rankine cycle (González-Mora and Durán-García, 2024).

This study evaluates the technical feasibility of a 10 MW high-temperature Kalina cycle (HT-KC) integrated with parabolic trough collectors (PTC) and a two-tank molten salt TES system under actual solar conditions in Mexico. We develop a detailed energy and exergy model of the entire system and simulate design-day and year-round performance. The goal is to quantify the solar fraction, capacity factor, and thermodynamic efficiencies achievable with this configuration and provide insights into its potential for practical deployment in Mexico's emerging CSP sector.

2. Materials and methods

2.1. System configuration

The system's core is a 10 MW high-temperature Kalina cycle (HT-KC) that uses an ammonia–water mixture optimized for efficient heat recovery at CSP-relevant temperatures (see Fig. 1). In the Heat Recovery Vapor Generator (HRVG), the working fluid is vaporized and then superheated before expanding through the turbine (stream 14) to produce mechanical work. The turbine exhaust (stream 13) is cooled in heat exchanger HX2 (exit as stream 15) and mixed with a lean ammonia solution (stream 4). This deliberate dilution raises the condensation temperature of the mixture, preventing high-ammonia concentrations from causing crystallization or corrosion in the absorber. The condensed liquid from HX2 (stream 18) is pressurized and then split: part (stream 20) passes through HX1 and HX2 to recover residual heat before entering the separator. The remainder (stream 19) mixes with ammonia-rich vapor (stream 6) to maintain the optimal working-fluid concentration.

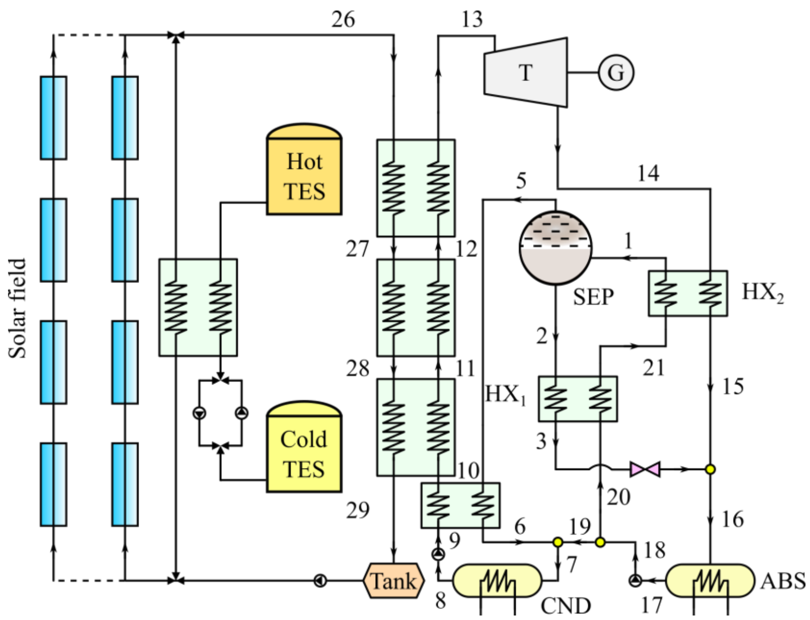

Fig. 1: Schematic diagram of the HT-KC

Inside the separator, the flow divides into ammonia-rich vapor (stream 5) and ammonia-lean liquid (stream 2). The lean liquid releases additional heat in HX1, is throttled to lower pressure (stream 4), and then absorbs heat from HX2 before final condensation. The rich vapor condenses (stream 8), is repressurized (stream 9), and returns to the HRVG via HX3—an integrated economizer, evaporator, and superheater train that prepares the fluid for the next cycle. By maximizing internal heat recovery in HX1, HX2, and HX3, and by carefully balancing dilution and concentration streams, the design minimizes exergy destruction and pumping work, thereby elevating the net power output and making the HT-KC particularly well suited to high-temperature CSP and industrial waste-heat applications.

Thermal energy is supplied to the HT-KC by a parabolic trough collector (PTC) field using Therminol VP1 as the heat transfer fluid (HTF). In this study, we selected Therminol VP1 for its low viscosity and stability up to 400°C (Therminoil, 2020). The field discharges into a two-tank molten-salt thermal energy storage (TES) system, using Solar Salt (60 wt% NaNO3, 40 wt% KNO3) that operates between 290°C (cold tank) and 565°C (hot tank) to minimize thermal losses (Steinmann, 2012). An intermediate heat recovery steam generator (HRSG) transfers energy from Therminol VP1 to the molten salt, maintaining each fluid within its optimal temperature window: the HTF maximizes solar absorption in the PTC array, while the molten salt provides high-density, dispatchable storage. This indirect coupling decouples heat collection from power generation, allowing the HT-KC to run continuously and stabilize output despite solar intermittency. In this study, we sized the TES capacity and charge/discharge rates to match the PTC field's daily energy yield and the HT-KC's 10 MW demand, thereby synchronizing solar availability, storage duration, and grid requirements.

2.2. Simulation framework and performance indicators

The design of the 10 MW HT-KC plant begins with determining the required thermal power input to the power block. We define the solar multiple (SM) as 1.5, which establishes the sizing of the solar field according to:

$$SM = \frac{\dot{Q}_{PB}}{\dot{Q}_{SF}} \qquad \text{(eq. 1)}$$

Here, SM is the ratio of the solar field's thermal output ($\dot{Q}_{SF}$) to the power block's thermal input ($\dot{Q}_{PB}$). Once $\dot{Q}_{PB}$ is known, the thermal power delivered by the PTCs is calculated as:

$$\dot{Q}_{PTC} = A_{ap} DNI \eta_o F_{soil} IAM - \dot{Q}_{loss} \qquad \text{(eq. 2)}$$

In this equation, A_{ap} denotes the PTC aperture area, η_o the optical efficiency, F_{soil} the soiling factor, IAM the incidence angle modifier, and $\dot{Q}_{loss}$ the total receiver thermal losses. We model a Eurotrough-type PTC with a 5.77 m aperture width and η_o=0.7554. Incidence angle modifier curves follow Zarza (2021), and we assume F_{soil}=0.92 to reflect continuous mirror cleaning. The design point is set at noon on 21 June, from which we derive the required solar field area.

Next, we determine the two-tank molten-salt TES volume by the HTF energy density (E_{TES}) and the required storage capacity:

$$V_{TES} = \frac{\dot{Q}_{SF} t_{storage}}{E_{TES}} \qquad \text{(eq. 3)}$$

To evaluate performance, we compute the following energy efficiencies:

- Solar field efficiency ($\eta_{I,SF}$) as the ratio of net thermal power transferred to the HTF ($\dot{Q}_{SF}$) to the incident solar power on the mirror aperture ($\dot{Q}_{inc}$) (Eq. 4a).
- Power block efficiency ($\eta_{I,PB}$) as the net power output ($\dot{W}$=10 MW) divided by $\dot{Q}_{SF}$ (Eq. 4b).
- Overall energy efficiency (η_I) that relates $\eta_{I,SF}$ and $\eta_{I,PB}$ (Eq. 4c).

$$\eta_{I,SF} = \frac{\dot{Q}_{SF}}{\dot{Q}_{inc}} \qquad \text{(eq. 4a)}$$

$$\eta_{I,PB} = \frac{\dot{W}}{\dot{Q}_{SF}} \qquad \text{(eq. 4b)}$$

$$\eta_I = \frac{\dot{W}}{\dot{Q}_{inc}} = \eta_{I,SF} \times \eta_{I,PB} \qquad \text{(eq. 4c)}$$

For exergy analysis, we use:

- Solar field exergy efficiency ($\eta_{II,SF}$) as the ratio of the HTF exergy gain ($\dot{Ex}_{SF}$) to the exergy of incident solar radiation ($\dot{Ex}_{inc}$), with $\dot{Ex}_{inc}$ computed via the MPD model (González-Mora et al., 2023) (Eq. 5a).
- Power block exergy efficiency ($\eta_{II,PB}$) as the net power output ($\dot{W}$=10 MW) divided by $\dot{Ex}_{SF}$ (Eq. 5b).
- Overall exergy efficiency (η_{II}) that relates $\eta_{II,SF}$ and $\eta_{II,PB}$ (Eq. 5c).

$$\eta_{II,SF} = \frac{\dot{Ex}_{SF}}{\dot{Ex}_{inc}} \qquad \text{(eq. 5a)}$$

$$\eta_{II,PB} = \frac{\dot{W}}{\dot{Ex}_{SF}} \qquad \text{(eq. 5b)}$$

$$\eta_{II} = \frac{\dot{W}}{\dot{Ex}_{inc}} = \eta_{II,SF} \times \eta_{II,PB} \qquad \text{(eq. 5c)}$$

3. Results

3.1. Kalina cycle characterization

The HT-KC was optimized using the Variable Metric Method to maximize overall exergy efficiency while adhering to key thermodynamic and operational constraints. We set the critical design parameters as follows:

- Turbine inlet: Ammonia–water mixture at 380 °C, 100 bar, concentration 0.75
- Separator: Held at 80 °C, splitting the flow into a vapor phase (concentration 0.97) and a liquid phase (concentration 0.40)
- Absorber feed: Strong solution at concentration 0.50 to maintain stable absorption performance
- Mechanical efficiencies: Turbine η=0.80, pump η=0.75
- HRSG terminal temperature difference: 10°C

Exergy streams for the ammonia–water mixture were calculated according to the Szargut method (2005), enabling precise quantification of exergy destruction in each component. Iterative refinements converged on a configuration balancing high turbine work output against minimized heat-exchanger losses. The tight 10 °C approach in the HRSG significantly curtailed entropy generation, improving cycle performance under realistic solar-thermal conditions.

Table 1 summarizes the optimized thermodynamic states at each point in the cycle. The resulting design achieves a favorable compromise between net power production and exergy utilization, demonstrating the HT-KC's versatility for integration with parabolic trough–driven heat sources. This characterization provides a robust framework for scaling the cycle in concert with solar field output, supporting technical feasibility and economic viability in CSP applications.

3.2. Design-day performance and typical-day performance

The design point is defined at solar noon on 21 June, corresponding to the maximum thermal output of the Eurotrough-like PTC field (4.06 m collector length). Under these conditions, the DNI, ambient temperature, and receiver inlet temperature reach annual peaks. Table 2 summarizes these design-day parameters. We size the solar field and two-tank molten-salt TES system to meet the HT-KC's thermal power requirement while ensuring turbulent flow in the receiver tubes for optimal heat-transfer coefficients.

To assess seasonal variability, we examine both equinox and solstice performance. Figures 2a and 2b plot the hourly thermal power delivered to the HTF alongside the corresponding energy and exergy efficiencies for representative "typical" days in March, June, September, and December. These profiles reveal how midday peaks attenuate in winter and autumn, and how the TES system buffers fluctuations by discharging stored heat during low-DNI periods.

Tab. 1: HT-KC thermodynamic states

State	P_i, (bar)	T_i, (C)	x_i	Q_i	h_i, (kJ/kg)	s_i, (kJ/kg·K)	ex_i, (kJ/kg)	$\dot{m}_i$, (kg/s)
1	9.457	80	0.5	0.1745	361.9	1.678	13.02	52.43
2	9.457	80	0.4	0	128	0.9948	-32.62	43.23
3	9.457	1.058	0.4	-0.001	-222.2	-0.1273	-32.45	43.23
4	3.013	1.211	0.4	-0.001	-222.2	-0.1246	-33.29	43.23
5	9.457	80	0.97	0.9947	1461	4.888	227.5	9.198
6	9.457	24.27	0.97	0.2036	331.8	1.219	243.8	9.198
7	9.457	35.14	0.75	0.1018	116	0.8394	91.36	17.29
8	9.457	33.11	0.75	0	-15.18	0.4147	92.83	17.29
9	100	35.52	0.75	-0.001	1.747	0.4284	105.5	17.29
10	100	150	0.75	-0.001	602.5	2.071	193.3	17.29
11	100	154.1	0.75	0	627.9	2.131	200.1	17.29
12	100	228.3	0.75	1	1871	4.806	608.1	17.29
13	100	380	0.75	1.001	2381	5.691	841.8	17.29
14	3.013	94.85	0.75	0.9995	1782	6.099	115.6	17.29
15	3.013	70.11	0.75	0.7415	1169	4.384	37.29	17.29
16	3.013	39.56	0.5	0.1594	175.2	1.208	-26.9	60.52
17	3.013	24.47	0.5	0	-130.4	0.2097	-20.89	60.52
18	9.457	24.57	0.5	-0.001	-129.4	0.2106	-20.13	60.52
19	9.457	24.57	0.5	-0.001	-129.4	0.2106	-20.13	8.094
20	9.457	24.57	0.5	-0.001	-129.4	0.2106	-20.13	52.43
21	9.457	67.97	0.5	0.0685	159.4	1.097	-8.265	52.43

Tab. 2: Desing conditions

Parameter	Symbol	Value
DNI, (W/m^2)	DNI	746
Ambient temperature, (ºC)	T_0	31.8
Location, (deg)	Φ_{loc}	20.88
Longitude, (deg)	L_{loc}	-103.84
HTF inlet temperature, (ºC)	T_{29}	290
HTF outlet temperature, (ºC)	T_{26}	390

Table 3 details solar field operating conditions for each typical-day scenario, including hourly DNI, HTF inlet/outlet temperatures, and molten-salt tank states. These results demonstrate that the combined PTC–TES–

HT-KC system maintains stable power output throughout the year, achieving above-design efficiency on summer days and leveraging stored thermal energy to stabilize winter and shoulder-season production.

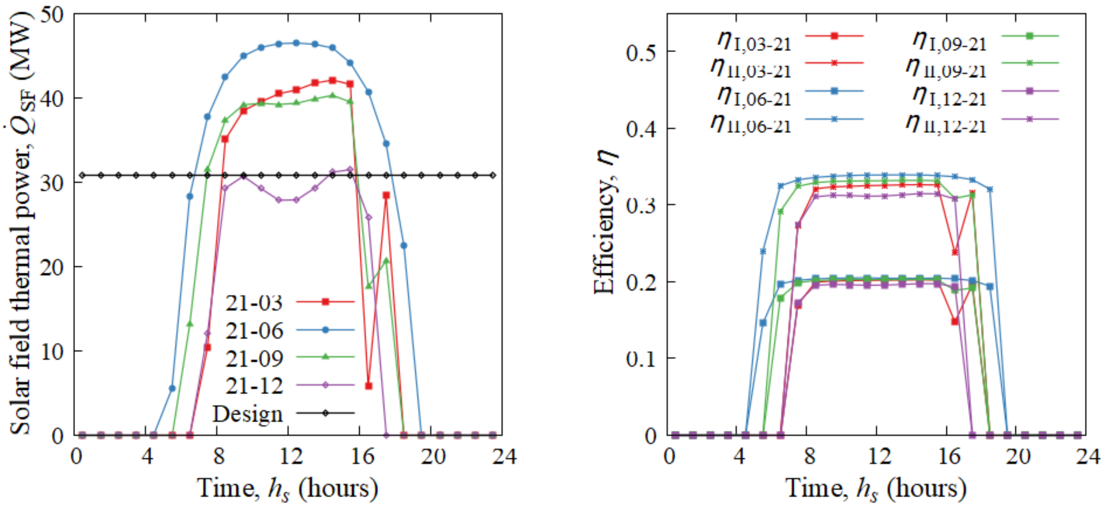

(a) Thermal power delivered by the solar field **(b) Efficiency of the HT-KC installation**

Fig. 2: Daily performance

Tab. 3: Solar field operating conditions

Parameter	Symbol	Value
Total mass flow rate, (kg/s)	$\dot{m}_{HTF}$	190.3
Flow velocity, (m/s)	u_∞	1.024
Reynolds number	Re	3.045×10^5
Operation time (h)	t_{op}	5.5
Number of loops	N_{loops}	62
Number of PTC per loop	N_{PTC}	52
Total concentration area, (ha)	A_{SF}	7.553
TES size, (m^3)	V_{TES}	1959

3.3. Annual performance

We conducted an hourly year-long simulation to capture daily and seasonal variations in DNI, ambient temperature, and incidence angle. The solar field aperture area, sized for the June 21 design point, remained constant, while $\dot{Q}_{loss}$, DNI, and the IAM were updated at each time step to reflect real-time environmental conditions. A constant soiling factor of 0.92 was assumed to represent continuous mirror maintenance.

Figure 3 shows the annual profile of thermal power delivered to the HTF. Pronounced diurnal cycles are evident, with peak outputs occurring during summer and significantly reduced deliveries in winter. This seasonal trend underscores the system's sensitivity to variations in solar resource and ambient conditions. Although the fixed sizing of the solar field and TES provides a stable performance baseline, the observed fluctuations highlight the importance of adaptive operational strategies—such as variable mass-flow control or adjustable thermal storage dispatch—to bridge seasonal energy shortfalls and maximize annual energy yield.

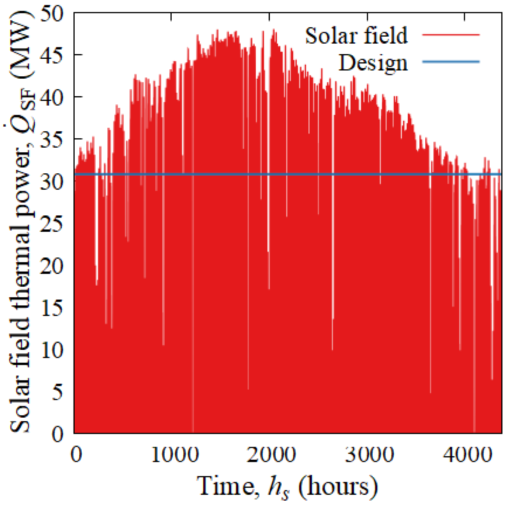

Fig. 3: Yearly performance

4. Discussion

The simulation results in Table 4 offer key insights into the HT-KC system's performance under Mexico's solar regime. During the equinoxes (21 March and 21 September) and the summer solstice (21 June), the system reaches its highest thermal power delivery and peak efficiencies at solar noon, reflecting the optimal alignment of solar geometry and collector orientation (Figs. 2a-c). By contrast, on the winter solstice (21 December), the lower solar elevation and shorter day length shift the peak efficiency to earlier in the morning. This seasonal asymmetry manifests in a solar fraction decline from 75.16 % in summer to 38.81 % in winter, and a two-hour reduction in daily operating hours relative to June.

On an annual basis, the fixed solar field (sized for 21 June) delivers 112.81 GWh of thermal energy, whereas the HT-KC requires 269.43 GWh, yielding a 41.87% solar fraction and a 44.10% capacity factor (Table 4). Both energy and exergy efficiencies remain remarkably stable—approximately 19% and 22%, respectively—demonstrating the cycle's robust thermodynamic design. However, these averages reflect the inherent losses from solar intermittency and TES round-trip inefficiencies.

On the design day (21 June), the HT-KC achieves its best performance metrics: a 75.16 % solar fraction, seven hours of continuous operation, and a 60.87% capacity factor (Table 4). In contrast, in December, the capacity factor falls to 43.48 %, with only five operating hours, underscoring the need for adaptive strategies—such as oversized fields or hybrid backup—to mitigate winter underperformance. Detailed component metrics in Table 4 confirm strong performance in high-irradiance seasons while highlighting areas for design refinement to address Mexico's pronounced seasonal variability.

A comparison with a 10 MW direct steam generation (DSG) Rankine cycle using the same parabolic trough field (González-Mora and Durán-García, 2024) reveals critical trade-offs. The DSG cycle attains higher first-law and exergy efficiencies—26% and 35%, respectively—versus 19% and 22% for the HT-KC. This gap arises because the HT-KC relies on an intermediate heat recovery steam generator to transfer energy from the Therminol-based solar field to the ammonia–water mixture, incurring additional exergy destruction. By contrast, the DSG approach generates steam directly in the PTC receivers, eliminating this extra heat-exchange stage.

However, the DSG configuration requires a larger solar field (7.74 ha vs. 7.55 ha for the HT-KC) and lacks cost-effective TES, limiting its dispatchability. Though slightly less efficient, the HT-KC integrates seamlessly with molten-salt storage to enable stable power output during non-solar periods, enhancing grid reliability. Thus, choosing between the two cycles involves prioritizing either peak thermodynamic efficiency (DSG) or operational flexibility and continuous renewable generation (HT-KC).

Agua Prieta, Sonora, exemplifies an ideal CSP site, with DNI exceeding 7.5 kWh/m^2/day and arid conditions favorable for dry cooling. Yet, deploying a standalone HT-KC plant—or retrofitting the existing Agua Prieta

II ISCC—is constrained by infrastructure incompatibilities and operational complexities. A new installation must leverage robust TES to counteract winter shortfalls. In this regard, the HT-KC's compatibility with molten salt storage offers a decisive dispatchability advantage over the DSG cycle, which struggles to integrate affordable storage despite its higher thermal efficiency.

Several technical challenges accompany Kalina cycle deployment: precise control of ammonia–water concentrations, demand for corrosion-resistant alloys, and specialized maintenance capabilities currently limited within Mexico's nascent CSP industry. Economically, the HT-KC's smaller land footprint may reduce site acquisition costs; however, its higher capital requirements for specialized heat exchangers and turbines could deter investors accustomed to conventional steam-cycle economics. Conversely, the DSG cycle benefits from established steam-cycle supply chains but cannot deliver 24/7 power without prohibitive TES investments.

Ultimately, Agua Prieta's abundant solar resource and growing energy demand support viable pathways for both cycles. The choice will hinge on Mexico's strategic objectives: the HT-KC offers long-term decarbonization and grid stability through integrated storage, whereas the DSG Rankine cycle delivers near-term efficiency gains. Achieving an optimal balance will require targeted policy incentives, localized feasibility studies, and collaborative partnerships to mitigate technical risks and align CSP deployments with regional energy transition and industrial goals.

Tab. 4: Summary of the HT-KC performance

Parameter	21 March	21 June	21 September	21 December	Year
Thermal energy delivered by the solar field	364.22 MWh	531.74 MWh	396.69 MWh	274.57 MWh	112.81 GWh
Thermal energy required to run the HT-KC	707.48 MWh				
Solar fraction	51.50 %	75.16 %	56.07 %	38.81 %	41.87 %
System operating hours	11 h	14 h	12 h	10 h	3863 h
Average energy efficiency	0.19	0.20	0.20	0.19	0.19
Average exergy efficiency	0.26	0.23	0.22	0.21	0.22
Capacity factor	47.83 %	60.87 %	52.17 %	43.48 %	44.10 %

5. Conclusions

This study assessed the technical feasibility and performance of a 10 MW high-temperature Kalina cycle (HT-KC) integrated with a parabolic trough collector (PTC) field and two-tank molten salt thermal energy storage (TES) under Mexico's solar conditions. Using a validated in-house thermal model, we conducted design-day (21 June) and full annual hourly simulations, optimized the cycle's exergy efficiency via the Variable Metric Method, and sized the solar field and TES to establish a 1.5 solar multiple at the design point. Performance indicators—including first-law and second-law efficiencies, solar fraction, and capacity factors—were quantified and benchmarked against a 10 MW direct steam generation Rankine cycle using the same PTC field.

Under peak design-day conditions, the HT-KC achieved a first-law efficiency of 32.51% and an exergy efficiency of 66.4%, while annual results yielded a 41.87% solar fraction and a 44.10% capacity factor. Seasonal analysis revealed significant swings—from a 75.16% solar fraction on the summer solstice to 38.81% on the winter solstice—underscoring the critical role of TES in mitigating winter deficits and maintaining a multi-hour operating window despite reduced DNI.

Key limitations of the current study include the assumption of a fixed solar field aperture—sized for 21 June and constant soiling and optical-loss factors, which may understate variations in winter performance and storage round-trip inefficiencies. Incorporating dynamic field sizing, variable soiling models, and real-time control of operating parameters could enhance predictive accuracy and operational resilience in future work.

By demonstrating the HT-KC's ability to integrate seamlessly with cost-effective molten salt storage, this research contributes novel insights into the trade-offs between thermodynamic complexity and dispatchability. Although conventional DSG Rankine cycles exhibit higher peak efficiencies (26% first-law, 35% exergy), they require larger solar fields and lack affordable TES options. Our findings provide a robust framework for designing and optimizing solar-driven Kalina cycles in high-irradiance regions and lay the groundwork for future studies on adaptive solar field strategies, hybridization with backup heat sources, cost-benefit analyses, and novel receiver designs to reduce indirect heat-exchange losses. These results inform plant developers and policymakers on the potential of HT-KC technology to deliver reliable, dispatchable renewable power in Mexico and similar climates.

6. Acknowledgments

This work was partially funded by COMECyT grant CAT2024-0112 (AESCo project), which supported Eduardo González-Mora through the *Programa Investigadoras e Investigadores*.

7. References

Bandhan, L.R., Rahman, Md.M., Aryan, S.A.D., Rana, Md.S., Akter, N., 2024. Assessing Efficient Waste Heat Recovery System for Marine Engine – A Thermodynamic Comparison of Organic Rankine Cycle and Kalina Cycle. SSRN Electronic Journal. https://doi.org/10.2139/ssrn.4854661

Elbir, A., 2024. Comparative analysis of Kalina and ORC cycles in renewable energy systems: exergo-environmental assessment and cost calculations with carbon emissions. International Journal of Energy Studies 9, 219–237. https://doi.org/10.58559/ijes.1449528

González-Mora, E., Durán-García, Ma.D., 2024. Assessing parabolic trough collectors and linear Fresnel reflectors direct steam generation solar power plants in Northwest México. Renew Energy 228, 120375. https://doi.org/10.1016/j.renene.2024.120375

González-Mora, E., Poudel, R., Durán-García, M.D., 2023. A practical upper-bound efficiency model for solar power plants. Journal of Non-Equilibrium Thermodynamics. https://doi.org/10.1515/jnet-2022-0080

Jeannot, I., Rahman, M.M., Saat, A., Faizal, H.M., Abdul Wahid, M., 2021. Thermodynamic Evaluation of a Solar Based Kalina Cycle, in: Proceedings of the International Conference on Industrial Engineering and Operations Management. IEOM Society International, Michigan, USA. https://doi.org/10.46254/AN11.20210134

Lovegrove, K., Stein, W., 2021. Chapter 1 - Introduction to concentrating solar power technology, in: Lovegrove, K., Stein, W.B.T.-C.S.P.T. (Second E. (Eds.), Woodhead Publishing Series in Energy. Woodhead Publishing, pp. 3–17. https://doi.org/https://doi.org/10.1016/B978-0-12-819970-1.00012-8

Moya, E.Z., 2021. Parabolic-trough concentrating solar power systems, in: Concentrating Solar Power Technology. Elsevier, pp. 219–266. https://doi.org/10.1016/B978-0-12-819970-1.00009-8

Nemati, A., Nami, H., Ranjbar, F., Yari, M., 2017. A comparative thermodynamic analysis of ORC and Kalina cycles for waste heat recovery: A case study for CGAM cogeneration system. Case Studies in Thermal Engineering 9, 1–13. https://doi.org/10.1016/J.CSITE.2016.11.003

NREL, 2023. Concentrating Solar Power Projects [WWW Document]. URL https://solarpaces.nrel.gov/by-technology (accessed 10.18.23).

Prieto, C., Cabeza, L.F., Pavón-Moreno, M.C., Palomo, E., 2024. Thermal energy storage for direct steam generation concentrating solar power plants: Concept and materials selection. J Energy Storage 83, 110618. https://doi.org/10.1016/J.EST.2024.110618

SENER, 2023a. Balance Nacional de Energía 2022.

SENER, 2023b. Atlas Nacional de Zonas con Alto Potencial de Energías Limpias.

SENER, 2017. Planta de Ciclo Combinado Agua Prieta II.

Steinmann, W.-D., 2012. 11 – Thermal energy storage systems for concentrating solar power (CSP) plants, in: Concentrating Solar Power Technology. pp. 362–394. https://doi.org/10.1533/9780857096173.2.362

Szargut, J., 2005. Exergy method: technical and ecological applications. WIT press.

Therminoil, 2020. Therminol Heat Transfer Fluids by Eastman [WWW Document]. URL https://www.therminol.com (accessed 9.17.20).